

Article

New Framework to Study Electromagnetic Turbulence

Mario J. Pinheiro 

Department of Physics, Instituto Superior Técnico, University of Lisbon, Avenida Rovisco Pais, 1049-001 Lisbon, Portugal; mpinheiro@tecnico.ulisboa.pt

Abstract: Combining a current source involving vortical surface currents in the set of Maxwell's equations offers a functional framework to address the complex phenomena of electromagnetic turbulence. The field structure equations exhibit fluid behavior with associated electromagnetic viscosity and reveal that the electromagnetic field, as a fluid, shows turbulent properties. This is an entirely new mechanism, investigated for the first time to the best of our knowledge. The fluidic–electromagnetic analogy implies that diffraction is the analog phenomenon of EM turbulence. The method clarifies the role of vortical surface currents in generating electromagnetic turbulence and classical fractal-like behavior in optical devices and suggests norms to design suitable plasmon circuitry to control electromagnetic turbulence in stealth technology and propulsion machines.

Keywords: electromagnetic turbulence; fluid dynamics; Maxwell's equations; propulsion; optical devices; stealth technology

1. Introduction

In 1883, Osborne Reynolds discovered the phenomenon of fluid dynamic turbulence when studying the flow of water in a cylindrical pipe driven by a pressure gradient. He found that when a critical velocity (well-characterized by a critical value of the so-called Reynolds number Re_c) was exceeded, the flow becomes turbulent. However, an absence of an adequate understanding of the origin of turbulence persists, outlasting a fundamental challenge to scientists and engineers as well, considering that most significant flows are turbulent.

Large-scale computational and experimental capabilities at the disposal of researchers and engineers certainly help in better comprehension and managing the source of turbulent flows. It is comprehended that turbulence is a random solenoidal motion of the fluid accompanied by a large increase of transport properties, such as viscosity (momentum), diffusivity (mass), heat conductivity (energy), and resistivity (electric current). The turbulent flow is energetically fed by the main flow, and energy losses may rise as a pressure drop or friction loss (with energy spectra $E(k) = C_K \epsilon^{2/3} k^{-5/3}$, according to Kolmogorov's theory), see Refs. [1,2]. Turbulence also occurs in conducting fluids (ionic flows) due to an interaction with the background electromagnetic field (radial profile of $\mathbf{E} \times \mathbf{B}$ shear flows at the edge of fusion device characterized by the gyrocenter shift induced by the collisions between ion and neutral [3,4]), and turbulent suppression is possible when the radial shearing rate of the $\mathbf{E} \times \mathbf{B}$ plasma flows, $\omega_{EB} = \frac{dv_{EB}}{dr}$ is of the order of the linear growth rate of the turbulent modes [5,6]. Understanding the effects of sheared flows is paramount for attaining a fusion reactor, in particular due to their typically beneficial effects upon plasma energy confinement and stability.

For an inviscid, ideally conducting fluid in the presence of an electromagnetic field, the magnetic field lines hook to the fluid [7]. If the fluid has a small resistivity, then the magnetic field lines will slowly diffuse through the medium [8]. If turbulence may be defined as the field of random or chaotic vorticity, then the noise may be defined as the random motion of boundaries [9]. Although there are some difficulties in defining turbulence, there seems to exist a consensus that turbulence evolution in a fluid is a thermodynamically irreversible



Citation: Pinheiro, M.J. New Framework to Study Electromagnetic Turbulence. *Magnetism* **2022**, *2*, 356–367. <https://doi.org/10.3390/magnetism2040025>

Academic Editor: Guido Ala

Received: 22 August 2022

Accepted: 13 October 2022

Published: 26 October 2022

Publisher's Note: MDPI stays neutral with regard to jurisdictional claims in published maps and institutional affiliations.



Copyright: © 2022 by the authors. Licensee MDPI, Basel, Switzerland. This article is an open access article distributed under the terms and conditions of the Creative Commons Attribution (CC BY) license (<https://creativecommons.org/licenses/by/4.0/>).

process [10–12]. Furthermore, according to von Karman [13] turbulence appears when fluid flows past solid surfaces or by the flow of layers of fluids with different velocities past or over one another [14].

The main focus of the present work is to treat the electromagnetic field as a fluid revealing turbulent property. For this purpose, we adequately introduced vortical structures in Maxwell's equations and associated them with the concept of electromagnetic viscosity. Later on, we examine the electromagnetic field's turbulent behavior *per se*. In this sense, we follow Marmanis' suggestion, that vorticity ($\mathbf{w} = \nabla \times \mathbf{u}$) and the Lamb vector ($\mathbf{l} = \mathbf{w} \times \mathbf{u}$) should be central to the theory of turbulence [15].

MHD formulations with an appropriated Ohm's law would offer a more self-consistent formalism, for a particular geometrical configuration, to the electromagnetic turbulence generated by the motion of electrically conductive eddies (e.g. [16,17]). However, in this work, we aim to contribute with physical insight into the electromagnetic turbulence from the standpoint of classical fields, supported by established analogies with turbulent hydrodynamics, especially highlighting the role of electric surface currents. The method gives access to an electromagnetic viscosity, clarifies the role of surface currents in generating electromagnetic turbulence and classical fractal-like behavior in optical devices [18,19], and suggests norms to design suitable plasmon circuitry to control electromagnetic turbulence in stealth technology [20,21] and propulsion machines [22,23].

1.1. Modification of Maxwell's Equations

Maxwell put the source current under the general form (as it follows from the Helmholtz's theorem):

$$\mathbf{C} = \mathbf{J} + \frac{\partial \mathbf{D}}{\partial t} + \text{curl } \mathbf{Z}, \quad (1)$$

with $\nabla \cdot \mathbf{C} = 0$, without specifying, or going further, on the characterization of the physical quantity Z . We can verify that this new field has the dimension of a surface density of current $[Z] = A/m$. Equation (1) encodes the Hodge–de Rham decomposition theorem for a regular p -form of degree p , which is a sum of exact, harmonic, and co-exact p forms.

Vorticity generates turbulence, and Stoke's theorem indicates that a local vortex pinned at a location will drag fluid in a rotating state, even in the case of a perfect fluid [24]. This effect is analog to the production of a magnetic field by a rectilinear current, a sort of *induction of velocity*. Vorticity is the seed of turbulence. The vortex starts to grow on a mixed layer of magnitude $\delta(y)$, where x is the distance relative to the point where the flowing starts, the leading edge. Consequently, we can assimilate the vortex as a kind of surface molecular current or eddy current. Eddy currents are dissipative processes. We will represent the structure of this vector field by the *Ansatz* \mathbf{M} , such as an associated induced current density $\mathbf{J}_{rot} = \text{curl } \mathbf{M}$, is created, introducing the magnetization vector field \mathbf{M} (with \mathbf{J}_{rot} in units A/m^2).

However, there exists a well-known relationship between the magnetization vector and the magnetic field intensity \mathbf{H} , $\mathbf{M} = \chi_m \mathbf{H}$, where χ_m is a dimensionless quantity called magnetic susceptibility, and $\mathbf{H} = \frac{1}{\mu} \mathbf{B}$, then we may write

$$\mathbf{J}_{rot} = -\frac{\chi_m}{\mu} \Delta \mathbf{A}, \quad (2)$$

since $\nabla \cdot \mathbf{A} = 0$, ensuring continuity in the current flow and $\mathbf{B} = \nabla \times \mathbf{A}$. It results from the above that the Ampère's equation should read instead:

$$c^2[\nabla \times \mathbf{B}] = \frac{\partial \mathbf{D}}{\partial t} + \mathbf{J} - \frac{\chi_m}{\mu} \Delta \mathbf{A}. \quad (3)$$

The previous Equation (3) appears (without the new term) more frequently under the form of Ampère's equation for vector \mathbf{H} :

$$\frac{\partial \mathbf{D}}{\partial t} = [\nabla \times \mathbf{H}] - \mathbf{J}, \quad (4)$$

after introducing a new excitation magnetic field $\mathbf{H} \equiv \mathbf{B}/\mu_0 - \mathbf{M}$. Equation (3) has a dissipative component in the last term. It allows a straightforward deduction of London's equation characterizing superconductors. Inside the sample $\mathbf{B} = 0$ and as \mathbf{E} arises from a changing magnetic field, then $\text{grad } V = 0$. So, Equation (3) gives straightforwardly

$$\nabla^2 \mathbf{A} - \frac{\mu}{\chi_m} \mathbf{J} = 0. \quad (5)$$

London admitted that the superconductor consisted in a condensation in a state of zero momentum, and hence:

$$\mathbf{P} = m\mathbf{v} + q\mathbf{A} = 0. \quad (6)$$

However, since $\mathbf{J} = nq\mathbf{v}$, then, from Equation (6), we obtain

$$\frac{m}{nq^2} \mathbf{J} + \mathbf{A} = 0. \quad (7)$$

Combining Equations (5)–(7) and noting that for a superconductor, $\chi_m = -1$, we obtain:

$$\nabla^2 \mathbf{A} - \lambda_L^2 \mathbf{A} = 0, \quad (8)$$

admitting the solution $\mathbf{A} = \mathbf{A}_0 \exp(-z/\lambda_L)$, with $\lambda_L^2 = \mu n q^2 / m \chi_m$ denoting the London penetration depth, the characteristic distance over which the field penetrates the superconductor. q is the effective charge of the carriers of the superconducting state (i.e., $q = 2e$, with $-e$ denoting the electron charge).

As shown in previous work [25] the electromotive force is given by:

$$\rho \mathbf{E} = -\rho \nabla \phi - \rho \frac{D\mathbf{A}}{Dt}. \quad (9)$$

Adding the term corresponding to the vortex structure, as subsumed in Equation (1), we introduce

$$\rho \mathbf{E} = -\rho \nabla \phi - \rho \frac{\partial \mathbf{A}}{\partial t} - \rho \nabla (\mathbf{v} \cdot \mathbf{A}) + \rho [\mathbf{v} \times \mathbf{B}] - n_s \frac{\hbar}{|e|} \nabla \times \mathbf{M}. \quad (10)$$

The last term on the r.h.s. contains two fundamental constants, \hbar and e , to secure homogeneity, and for consistency with the quantization of the magnetic flux. Notice that in superconductors, we have the flux given by Φ quantized according to $\frac{e\Phi}{\hbar c} = 2\pi n$, ($n = 0, \pm 1, \pm 2, \dots$), with n_s being the surface density of vortices filling the texture on the boundary layer above the blunt-body. The rationale of this simple choice is confirmed when compared with known phenomena. Using the relations $\mathbf{M} = \chi_m \mathbf{H}$ and $\mathbf{H} = \frac{1}{\mu} \text{curl } \mathbf{A}$, we finally obtain:

$$\frac{\partial \mathbf{A}}{\partial t} = \frac{\mathbf{F}^{ext}}{\rho} - \nabla \phi - \nabla (\mathbf{v} \cdot \mathbf{A}) + [\mathbf{v} \times \mathbf{B}] + v_{em} \Delta \mathbf{A}. \quad (11)$$

1.2. The Electromagnetic Viscosity Term

From the above Equation (11) we are required to define

$$v_{em} \equiv \frac{\hbar}{\rho} \left(\frac{n_s \chi_m}{|e| \mu} \right), \quad (12)$$

that plays the role of an *electromagnetic viscosity*, provided we replace $\mathbf{E} = [\mathbf{v} \times \mathbf{B}]$, a result also proposed by Marmanis in his Thesis [26].

The introduction of the electromotive force in connection with the convective (total) derivative drives us directly to the specific condition, which must be satisfied by \mathbf{B} . Taking the rotational of Equation (11) and not regarding external forces, is straightforwardly taken the following expression (e.g., [27]):

$$\frac{\partial \mathbf{B}}{\partial t} = \text{curl} [\mathbf{v} \times \mathbf{B}] + \eta \Delta \mathbf{B}, \quad (13)$$

where η is the resistivity of the medium, and it is equivalent to the magnitude obtained earlier, that is, $\eta \equiv v_{em}$. Equation (13) is the induction equation for the magnetic field in magnetohydrodynamics. In MHD this is taken to be $\eta = m_e \langle v_{ei} \rangle / n_e e^2$ in SI units, where μ_0 is the magnetic permeability. In order for the analogy to be completed, we have $\eta \equiv n_s \hbar / e \rho$, with $\rho = ne$, or

$$\eta = \frac{n_s \hbar}{n_v e^2 \chi_m}. \quad (14)$$

This result attests to the nature of the electric resistivity depending on the prefactor n_s/n_v , which shows its dependency from the electrons surface density, that without electrons present on a sheath-layer, no electromagnetic turbulence is achievable. Still, Equation (14) must be valid when analyzing an electromagnetic wave incident to an obstacle, when light passes through an aperture and the formed diffraction pattern.

Using the Bohm sheath criterion, where ions are supposed to leave the sheath with speed u_s above the Bohm speed $u_B = \sqrt{\frac{ek_B T_e}{M}}$, such as $u_s \geq u_B$, and considering that the potential drop Φ_p across the sheath-presheath launch the ions until they reach the Bohm speed, $Mu_B^2/2 = e\Phi_p$, we have $\Phi_p = T_e/2$, delivering to us a thumb rule for the ratio of the density at the sheath edge n_s over the density in the plasma n_v , such as $n_s \approx \frac{25}{41} n_v$ (see, e.g., Ref. [28]). Hence, in normal conditions, we may expect that the resistivity of the medium may have a maximum value:

$$\eta \leq \frac{n_s \hbar}{n_v e^2 \chi_m}. \quad (15)$$

The Bohm sheath theory should be valid in a nonequilibrium plasma at a sufficiently large energy scale. The local balance of kinetic energy conserves independently of the type of dominant forces, molecular in fluids or electromagnetic in plasma. Liouville's theorem imposes the trend on a bunch of particles in the phase space [29,30]. The Equation (15) implies that higher magnetic susceptibilities χ_m contribute to a substantial increase of the electric resistivity of the medium, typical in ferrimagnetic substances exhibiting high values of χ_m , and high electrical resistivity. Additionally, insulants, only possessing more increased surface charge density than volume charge, can hold high electric resistivity.

Conversely, Equation (14) gives for the surface density:

$$n_s = \frac{m_e \langle v_{ei} \rangle \mu}{\hbar \chi_m}. \quad (16)$$

In a typical plasma, we have $\langle v_{ei} \rangle \approx 10^9 \text{ s}^{-1}$ and for electrons we got $n_s \approx 10^3 / \chi_m$ particles/cm². For example, for hydrogen $\chi_m \approx 10^{-9}$ and $n_s \approx 10^{12}$ electrons per cm². The obtained expression for the electromagnetic viscosity scales well with the (magnetic diffusion based) Sweet-Parker sheet-model, $\tau = L^2 / \eta$, with L representing a field diffusion region, for example, $L \approx 10^4 \text{ km}$ in a solar flare [31]. Our estimated value for χ_m gives a too much longer time of reconnection in a solar flare, typically of the order of tens of minutes. However, a possible discrepancy may have originated on the physical mechanism related that emerges from the presence of the Planck's constant \hbar and the magnetic susceptibility χ_m in Equation (15).

Therefore, we may consider Equation (11) and, using the fluidic electrodynamics analogy, write the Navier–Stokes equation:

$$\frac{\partial \mathbf{u}}{\partial t} = -\nabla p - (\mathbf{u} \cdot \nabla \mathbf{u}) + \nu \Delta \mathbf{u}. \tag{17}$$

1.3. Time Rate of Magnetic Reconnection

The preceding arguments lead to the construction of a new expression for the viscosity, in terms of the superficial density of the fluid, and bulk density, as the critical ratio. One immediate advantage attained with this model stays in the important separation between the two groups of electrons, let us say, the normal (bulk) electrons n_v and the surface electrons n_s (that emerge at the surface of the medium, in the plasma sheet), and the total density of conduction electrons is $n = n_s + n_v$. Equation (13) provides us with a new formula for the time decay for a magnetic field (diffusion time):

$$\tau \simeq \frac{n_v}{n_s} \frac{e^2 L^2 \mu}{\hbar \chi_m}. \tag{18}$$

Here, L is a global length scale of change in the magnetic field. From Equation (18) we obtain an estimate for the time rate of magnetic reconnection, $\tau \approx 10^9$ years, assuming $n_v = 10^{12}$ electrons per cubic centimeter, and $n_s = 0.1n_v$. However, the term χ_m may become negative (and growing in magnitude) in an ideal plasma dominated by the diamagnetic effect of the charged particles in their helical trajectory around the magnetic field lines (see, e.g., Ref. [32]). As the forward Equation (21) shows, for a negative value of χ_m a spontaneous instability appears leading to $|\mathbf{A}| \sim e^{\eta k^2 t}$ for wavenumber k . Now, a plasma in pressure–balance equilibrium is perfectly diamagnetic (see, e.g., Refs. [33,34]), a state of generalized zero vorticity and helicity, the ends of the loop anchored in the dense photosphere, and this is the first state of minimum energy before the kink instability surging from a highly twisted flux rope evolves to a coronal mass ejection [35], the large eruption of plasma and magnetic fields from a star leading to the destruction of excess energy.

2. Spiral Structures and Turbulence

Equation (13) can be compared with the dynamical equations describing the fields the vorticity ω and Lamb vector \mathbf{l} :

$$\frac{\partial \omega}{\partial t} = -[\nabla \times \mathbf{l}] + \nu \nabla^2 \omega \tag{19}$$

and also

$$\nabla \cdot \omega = 0. \tag{20}$$

can be the analogue of $\nabla \cdot \mathbf{B} = 0$. Equation (19) is equivalent to the equation of conservation of angular momentum [36]. It can be shown that the parallel component of the angular momentum is conserved in a fully developed turbulence, result encoded in the Loitsyansky-like integral $I_{\parallel} = - \int r_{\perp}^2 \langle \mathbf{u}_{\perp} \cdot \mathbf{u}'_{\perp} \rangle d\mathbf{r}$, with $\langle \mathbf{u} \cdot \mathbf{u}' \rangle$ denoting the usual two-point velocity correlation and \perp indicating the component perpendicular to the external magnetic field [37]. It is a cornerstone in treating turbulence.

Equation (11) results in a diffusion type equation for each component of the vector potential field \mathbf{A} (in a rest-frame, $\mathbf{v} = 0$) that comes out from the modified Ampère’s Equation (4):

$$\frac{\partial \mathbf{A}}{\partial t} = \nu_{em} \nabla^2 \mathbf{A} + \mathbf{s}(\mathbf{r}, t). \tag{21}$$

The theory of turbulence in fluids is primarily founded on the flow representation of the vorticity field. Hence, we expect from Equation (21) to obtain a valid representation of the EM turbulence. We know that diffraction through an aperture can be explained through Faraday’s induction law [38], using Equation (13). We propose here an additional vectorial

source term $\mathbf{s}(\mathbf{r}, \mathbf{t})$, which might represent an incident electromagnetic wave hitting an obstacle. Remark that there is a field penetration depth, $\lambda_L = \sqrt{\frac{v_{em}}{f}}$, correlated to an electromagnetic wave with frequency f , which typically fall in the nanoscale (near-field) region. We intend to establish an analogy between both hydrodynamic and EM fields to solve problems in both fields, recommended by the similarity between Equations (19) and (21).

From a parabolic partial differential equation, like Equation (21), we can obtain a hyperbolic partial differential equation applying directly to the following field dependency

$$\mathbf{A}(x, y, z, t) = \mathbf{A}(x, y, z)T(t), \quad (22)$$

which is convenient for individual radiation sources, and obtaining a Sturm–Liouville type of equation where the electromagnetic theory matches the geometrical optics, according to the Sommerfeld and Runge approach [39]

$$\nabla^2 \mathbf{A}(\mathbf{r}) + k^2 \mathbf{A}(\mathbf{r}) = \delta(\mathbf{r}). \quad (23)$$

Here, $k = \sqrt{\epsilon\mu}\omega = 2\pi/\lambda$ is a constant in a given medium, and, for consistency with the above described framework, we should put $\omega = v_{em}k^2$ (as noticed before, v_{em} has the dimension $[L]^2/[T]$).

Controlled Electromagnetic Turbulence

Hence, the framework outlined above suggests that the solution of Equation (23) represents the turbulent vector potential and that diffraction is the analog phenomena of EM turbulence. Besides, it shows that the surface density of plasmons present on the obstacle to the waves impacts the diffraction phenomena. The solution of Equation (23) is given by (see Ref. [40])

$$\mathbf{A}(\mathbf{r}) = \frac{1}{4\pi} \iiint_{\infty} [\mu_0 \mathbf{J}_{\perp e}(\mathbf{r}') + \epsilon_0 \mathbf{J}_{\perp m}(\mathbf{r}')] \frac{e^{i\sqrt{\frac{\omega}{v_{em}}}|\mathbf{r}-\mathbf{r}'|}}{|\mathbf{r}-\mathbf{r}'|} d^3\mathbf{r}', \quad (24)$$

where $\mathbf{A}(\mathbf{r}, t) = \mathbf{A}(\mathbf{r})e^{i\omega t}$, and $\mathbf{J}_{\perp m, e}(\mathbf{r}')$ represent the transversal (electric and magnetic) current densities. It points out the action of scalar and vectorial waves on diffraction effects when an electromagnetic wave interacts with a surface layer of a material [41] (surface plasmons) or plasma, and to the possibility to control diffraction, aiming, for example, to enhance its intensity through gratings, or stealth technology, utilizing an appropriate combination of material properties and the light wave incident on its surface. Radiating EM waves are fed only by the transverse part of the current density, the source of the vector potential.

Could an array change its reflectivity by optimally grading the density of surface plasmons? This feature is feasible if conditions i) $k \gg 1/R$, $R \gg \lambda$, and ii) $z \approx R$ hold, then we rewrite for the plan $z > 0$

$$\mathbf{A}(x, y, z) = \frac{1}{4\pi} \iiint_{\infty} [\mu_0 \mathbf{J}_{\perp e}(\mathbf{r}') + \epsilon_0 \mathbf{J}_{\perp m}(\mathbf{r}')] e^{i[u_1(x-x') + u_2(y-y')] + iz\sqrt{k^2 - u_1^2 - u_2^2}}/R d^3\mathbf{r}' \quad (25)$$

with $R = \sqrt{(x-x')^2 + (y-y')^2 + z^2}$. Equation (24) is valid for a monochromatic wave, but using the superposition principle, we can construct a more general solution of the wave equation that includes plane waves with different amplitudes, phases and directions. Let us denote by α and ϕ the direction of propagation of the wave, with $k_x = u_1 = k \sin \alpha$

and $k_y = u_2 = k \cos \alpha \sin \phi$, and assume that the plan (x, y) is coplanar to the diffraction structure. Equation (25) becomes (for $z > 0$):

$$\mathbf{A}(x, y, z) = \frac{1}{4\pi^2} \iiint_{-\infty}^{\infty} \mathbf{g}(u_1, u_2) e^{i[u_1(x-x') + u_2(y-y')] + iz\sqrt{k^2 - u_1^2 - u_2^2}} du_1 du_2. \quad (26)$$

setting the wave plan distributions of amplitudes and phases in all directions, and with

$$\mathbf{g}(u_1, u_2) = \iint_{-\infty}^{\infty} \mathbf{A}(x', y', 0) e^{-i[u_1(x-x') + u_2(y-y')]} dx' dy' \quad (27)$$

representing the field angular spectra, build on the transversal current densities, and sit on the surface. Consider the relevant case when the field doesn't depend on coordinate y , such as $\mathbf{A}(x, y, z) = \mathbf{A}(x, 0, z)$, where the source is located only along the Ox axis.

Then,

$$g(u_1, u_2) = \iint \mathbf{A}(x', 0) e^{i[u_1(x') + u_2(y')]} dx' dy' = 2\pi \delta(u_2) g(u_1) \quad (28)$$

with

$$\mathbf{g}(u_1) = \int_{-\infty}^{\infty} \mathbf{A}(x', 0) e^{iu_1(x')} dx'. \quad (29)$$

The vector potential becomes:

$$\mathbf{A}(x, 0, z) = \frac{1}{2\pi} \int_{-\infty}^{+\infty} g(u) e^{iz\sqrt{k^2 - u^2}} e^{iux} du. \quad (30)$$

Applying the method of stationary phase, the vector potential can be written under the form (with \mathbf{i} denoting the unit vector along the Ox axis, and also \mathbf{j} and \mathbf{k}):

$$\mathbf{A}(x, 0, z) = \frac{1}{2\pi} g(u_0) e^{if(u_0) \mp \frac{\pi}{4}} \sqrt{\frac{2\pi}{\mp f''(u_0)}} e^{i\omega t} \mathbf{i} \quad (31)$$

with

$$f(u) = -z \sqrt{\frac{\omega}{v_{em}} - u^2} + ux. \quad (32)$$

After multiplying by the independent temporal term (according to Equation (22)) with

$$u_0 = \pm \frac{x}{\sqrt{x^2 + z^2}} \frac{\omega}{v_{em}}, \quad (33)$$

for the condition $f'(u_0) = 0$, and defining $f(u)$ such as:

$$f(u_0) \equiv -z \sqrt{k^2 - u_0^2} + u_0 x. \quad (34)$$

The variation of the wave number u that is related to phase variation of $f(u)$ from 0 to π is given by:

$$\Delta u = \sqrt{2\pi / (\mp f''(u_0))}. \quad (35)$$

The signs \mp in front of $f''(u_0)$ must be chosen for the argument of the square root to be positive, and $\mathbf{g}(u_0)$ is the angular spectrum of the wave field.

Finally, Equation (31) is written under the form:

$$\mathbf{A}(x, 0, z) = \frac{1}{2\pi} g(u_0) \sqrt{\frac{2\pi\omega}{v_{em}}} e^{i\omega t} \frac{z}{(x^2 + z^2)^{3/4}} e^{if(u_0) \mp \frac{\pi}{4}} \mathbf{i}. \quad (36)$$

Then, the conditions for anti-reflectivity, or superluminescence, are obtained. The maximum and minimum intensity A patterns are observed within the following conditions (where n is an integer), x_n expressing the position on the Ox axis of the n radiation sources:

$$\mathbf{A}(x, 0, z) = \begin{cases} A = 0, & \text{for } x_n = \pm \pi(n + \frac{1}{2}) \frac{v_{em}}{\omega}, \\ A = A_{max}, & \text{for } x_n = \pm 2\pi n \frac{v_{em}}{\omega} \end{cases} \quad (37)$$

The electric field can be calculated, giving

$$\mathbf{E} = \frac{\partial \mathbf{A}}{\partial t} = \frac{1}{2\pi} g(u_0) i\omega e^{i\omega t} \sqrt{\frac{2\pi\omega}{v_{em}}} e^{if(u_0) \mp \frac{\pi}{4}} \frac{z}{(x^2 + z^2)^{3/4}} \mathbf{i}, \quad (38)$$

and the magnetic field is

$$\mathbf{B} = \nabla \times \mathbf{A} = \frac{1}{2\pi} g(u_0) e^{i\omega t} \sqrt{\frac{2\pi\omega}{v_{em}}} e^{if(u_0) \mp \frac{\pi}{4}} \left[\frac{x^2(2 - 2i\sqrt{\frac{\omega}{v_{em}} \frac{xz}{\sqrt{x^2+z^2}}}) + z^2(-1 - 2i\sqrt{\frac{\omega}{v_{em}} \frac{xz}{\sqrt{x^2+z^2}}})}{2(x^2 + z^2)^{7/4}} \right] \mathbf{k}. \quad (39)$$

Figure 1a,b illustrate the effect of an applied electromagnetic wave of frequency ω acting on plasmons present on one point-like nanodevice, with one surface layer with n_s surface electrons density, sit on a metallic surface, or plasma, with n_v volumetric electron density. An EM wave with frequency ω actuates on electrons that shine modulated light above and below the nanodevice. It is assumed $z \ll 1$ in the numerical calculations shown in Figures 1a and 2b, representing the intensity of the emitted light $I = \langle |\mathbf{E}\mathbf{H}| \rangle$, with the Poynting vector, $\mathbf{S} = \frac{1}{\mu} \mathbf{E}\mathbf{B}$, including only the real part of the fields. We may notice that the Poynting vector aligns along the vertical axis, despite the EM momentum confined to a restricted volumetric region, with a maximum adjacent to the surface. The intensity distribution inside the thin surface layer where the EM viscosity is built-up is due to the plasmons vortex generating the effect of surface EM waves, that develop in multiple beam-like structures, depending on the ratio ω/v_{em} , as portrayed in Figure 2a,b, with evidence of turbulent, classical fractal-like behavior [42], when $\omega/v_{em} \gg 1$, with similarity to a transition to turbulence in the boundary layers. The scattered waves do not progress isotropically, but are transmitted or reflected, bordering along with the device structure. Similar streamwise vorticity fluctuations induced by near-wall vortices are visible in tubular structures in plane channel flows [43].

In the natural world, a multifunctional, angle-dependent anti-reflection structure occurs on cicada wings. The insect's wings are composed of highly ordered, tiny vertical "nano-nipple" arrays, forming a biomorphic TiO₂ surface with small spaces between the ordered nano-antireflective structures allowing multiple reflective and scattering effects of the antireflective structures [44]. Another recent technique revealing the role of surface charges on cloaking and shielding was proposed using electroosmotic dipole flow that occurs around a localized surface charge domain under the application of an external electric field in a Hele-Shaw cell, revealing that the superposition of surface charge spots does produce complex flow patterns, without the application of physical walls [45].

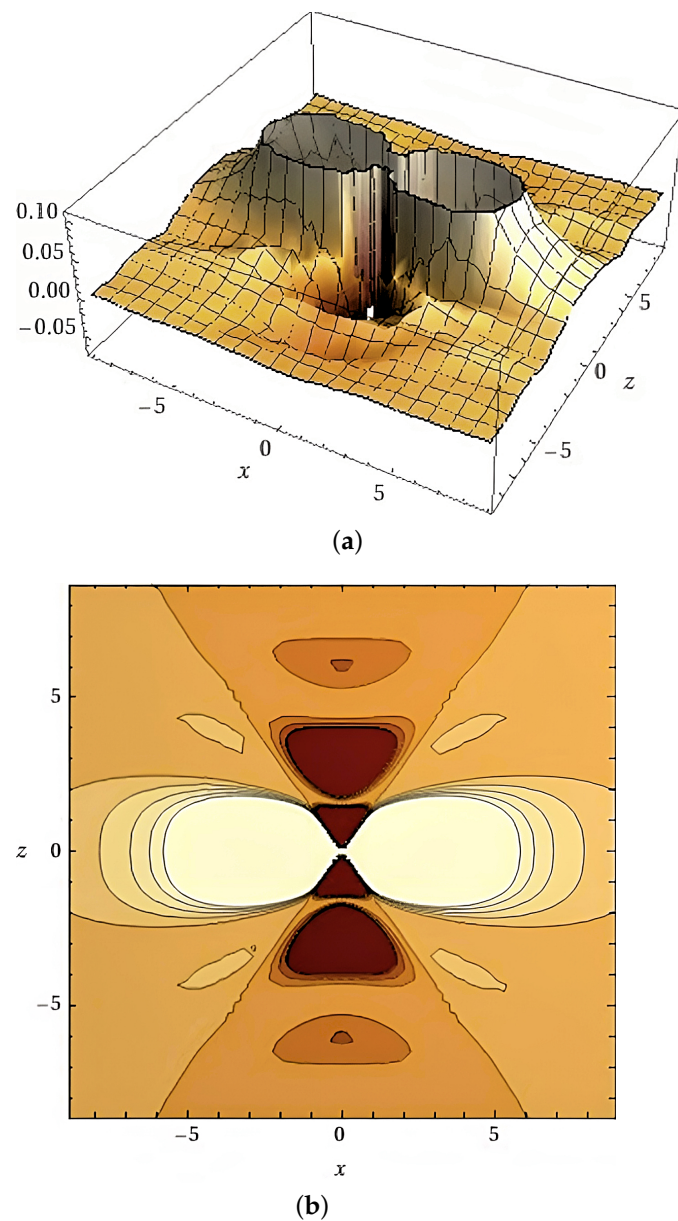
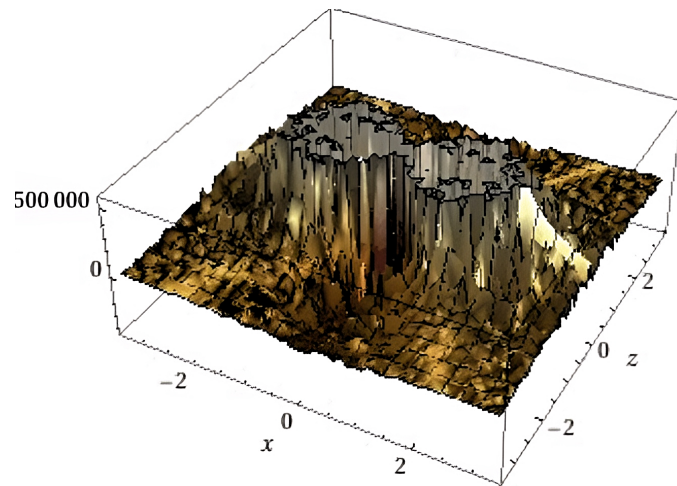
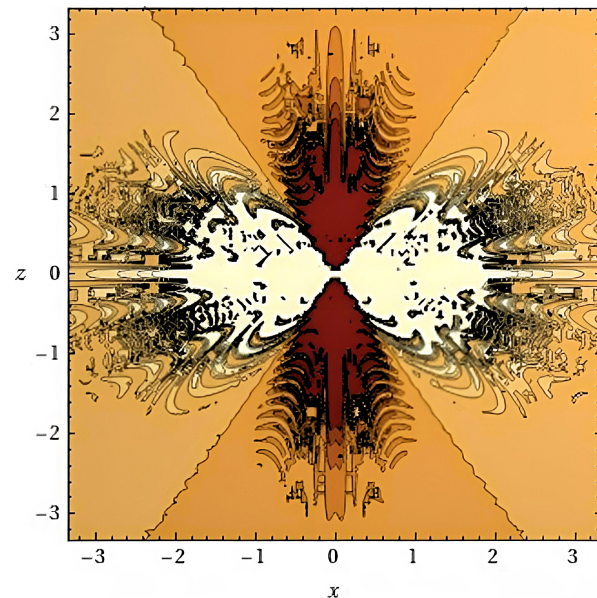


Figure 1. (a) 2D plot of the EM intensity distribution (in a.u.) below and above the device surface, $\omega/v_{em} = 3.1$; (b) contour plot of the EM intensity distribution at $y = 0$.

In stealth technology, we also may use a programmable plasmonic circuit, as was proposed in Ref. [46], using a transparent patterned zinc oxide gate to provide full control of plasmons in graphene. These techniques may assist in better design stealth technology [47], and Figure 3 exemplifies the concept. As wide spectrum surveillance (wide bandwidth capability) is needed because the frequency of the enemy radar is not known beforehand, the parameter v_{em} may be adjusted to lock with the enemy frequency radar ω [48].



(a)



(b)

Figure 2. (a) 2D plot of the EM intensity distribution (in a.u.) below and above the device surface, $\omega/v_{em} = 10^5$; (b) contour plot of the EM intensity distribution at $y = 0$.

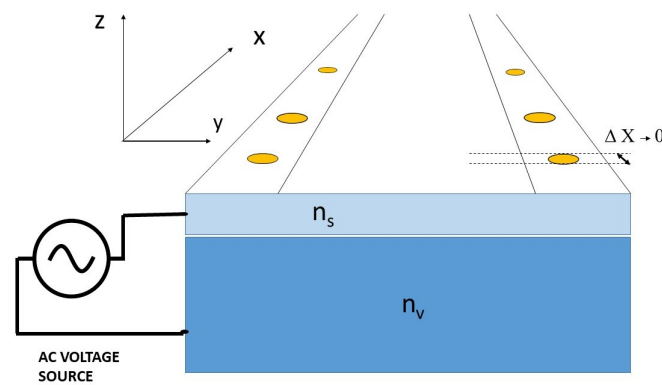


Figure 3. Plasmon circuit to induce electromagnetic amplification or attenuation. In the Fraunhofer diffraction (in the far-field region) analyzed here, in the far-field region, Δx determines the possible extent of the source, or pillar, as in cicada wings, here discussed as a punctual source.

3. Conclusions

The above scaling and methodology, based on the hydrodynamic construct of the electromagnetic field, introduces a new tool to assess electromagnetic turbulence or practical means to control optical phenomena such as cloaking and shielding and further reveals the diffraction nature of EM turbulence. The method gives access to an electromagnetic viscosity, clarifies the role of surface currents in generating electromagnetic turbulence and classical fractal-like behavior in optical devices, and suggests norms to design suitable plasmon circuitry to control electromagnetic turbulence in stealth technology and propulsion machines. The diffraction pattern is dependent not only on the form of the encountered barriers but, additionally, is essentially linked to the surface density of surface plasmons vortices and electrons being on the obstacle.

Funding: This research received no external funding.

Conflicts of Interest: The author declares no conflict of interest.

References

1. Tsytovich, V.N. Development of the Concepts of Plasma Turbulence. *Sov. Phys. Usp.* **1973**, *15*, 632. [[CrossRef](#)]
2. Marsch, E. Kinetic Physics of the Solar Corona and Solar Wind. *Living Rev. Sol. Phys.* **2006**, *3*, 1–100. [[CrossRef](#)]
3. Krommes, J.A. The Gyrokinetic Description of Microturbulence in Magnetized Plasmas. *Annu. Rev. Fluid Mech.* **2012**, *44*, 175–201. [[CrossRef](#)]
4. Antoni, V.; Spada, E.; Vianello, N.; Spolaore, M.; Cavazzana, R.; Serianni, G.; Martines, E. Shear flows generated by plasma turbulence and their influence on transport. *Plasma Phys. Control. Fusion* **2005**, *47*, B13. [[CrossRef](#)]
5. Biglari, H.; Diamond, P.H.; Terry, P.W. Influence of sheared poloidal rotation on edge turbulence. *Phys. Fluids B* **1990**, *2*, 1–4. [[CrossRef](#)]
6. Burrell, K.H. Effects of EB velocity shear and magnetic shear on turbulence and transport in magnetic confinement devices. *Phys. Plasmas* **1997**, *4*, 1499–1518. [[CrossRef](#)]
7. Keith, W.; Heikkila, W. *Earth's Magnetosphere Formed by the Low-Latitude Boundary Layer*; Academic Press: London, UK, 2021.
8. Hagelaar, G.J.M.; Oudini, N. Plasma transport across magnetic field lines in low-temperature plasma sources. *Plasma Phys. Control. Fusion* **2011**, *53*, 124032. [[CrossRef](#)]
9. Saffman, P.G. Weak interactions and coherent structures in turbulence. In *Transition and Turbulence*; Meyer, R.E., Ed.; Academic Press: New York, NY, USA, 1981.
10. Kiehn, R.M. Instability Patterns, Wakes and Topological Limit Sets. In *Eddy Structure Identification in Free Turbulent Shear Flows. Fluid Mechanics and Its Applications*; Bonnet J.P., Glauser M.N., Eds.; Springer: Dordrecht, The Netherlands, 1993; Volume 21.
11. Wu, W.; Wang, J. Nonequilibrium thermodynamics of turbulence and stochastic fluid systems. *New J. Phys.* **2020**, *22*, 113017. [[CrossRef](#)]
12. Martyushev, L.M. Maximum entropy production principle: History and current status. *Physics-Uspokhi* **2021**, *64*, 558. [[CrossRef](#)]
13. Rao, S. Modeling of Turbulent Flows and Boundary Layer. In *Computational Fluid Dynamics*; OH, H.W., Ed.; Books on Demand: Norderstedt, Germany, 2010; p. 285.
14. Kadivara, M.; Tormey, D.; McGranaghan, G. A review on turbulent flow over rough surfaces: Fundamentals and theories. *Int. J. Thermofluids* **2021**, *10*, 100077. [[CrossRef](#)]
15. Marmanis, H. Analogy between the Navier–Stokes equations and Maxwell's equations: Application to turbulence. *Phys. Fluids* **1998**, *10*, 1428–1437. [[CrossRef](#)]
16. Stawarz, J.E.; Matteini, L.; Parashar, T.N.; Franci, L.; Eastwood, J.P.; Gonzalez, C.A.; Gingell, I.L.; Burch, J.L.; Ergun, R.E.; Ahmadi, N.; et al. Comparative analysis of the various generalized Ohm's law terms in magnetosheath turbulence as observed by Magnetospheric Multiscale. *JGR Space Phys.* **2021**, *126*, e2020JA028447. [[CrossRef](#)]
17. Goedbloed, H.; Keppens, R.; Poedts, S. *Magneto-hydrodynamics of Laboratory and Astrophysical Plasmas*; Cambridge University Press: Cambridge, UK, 2019.
18. Gao, X.-Z.; Pan, Y.; Zhao, M.-D.; Zhang, G.-L.; Zhang, Y.; Tu, C.; Li, Y.; Wang, H.-T. Focusing behavior of the fractal vector optical fields designed by fractal lattice growth model. *Opt. Express* **2018**, *26*, 1597–1614. [[CrossRef](#)] [[PubMed](#)]
19. Pan, Y.; Gao, X.-Z.; Zhang, X.; Zhao, J.-H.; Zhao, P.-C.; Li, Y.; Tu, C.; Wang, H.-T. Diffraction properties and applications of spatially structured optical fields with fractal amplitude masks. *Appl. Opt.* **2019**, *58*, 8631–8637. [[CrossRef](#)] [[PubMed](#)]
20. He, Q.; Sun, S.L.; Xiao, S.Y.; Li, X.; Song, Z.Y.; Sun, W.J.; Zhou, L. Manipulating electromagnetic waves with metamaterials: Concept and microwave realizations. *Chin. Phys. B* **2014**, *23*, 047808. [[CrossRef](#)]
21. Lin, L.G.; Jian, T.; Hong, W.S. Research on Stealth Aircraft Control Circuit and Realization of Software Radio. *IOP Conf. Ser. Mater. Sci. Eng.* **2018**, *439*, 052021. [[CrossRef](#)]
22. Mathur, S.; Mukhtar, A. Achieving near light speed to faster than light speed via wave propagation and electromagnetic field propulsion. *Aeron Aero Open Access J.* **2021**, *5*, 103–106.

23. Lee, H.Y.; Kwak, M.S.; Lim, Ky.; Ahn, H.S.; Hwang, G.-T.; Ha, D.H.; Taylor, R.A.; Yi, S.N. Harvesting electrical energy using plasmon-enhanced light pressure in a platinum cut cone. *Opt. Express* **2021**, *29*, 35161–35171. [[CrossRef](#)]
24. Lesieur, M. *La Turbulence*; Press Universitaires de Grenoble: Grenoble, France, 1994; p. 39.
25. Martins, A.A.; Pinheiro, M.J. Fluidic electrodynamics: Approach to electromagnetic propulsion. *Phys. Fluids* **2009**, *21*, 097103. [[CrossRef](#)]
26. Marmanis, H. Analogy between the Electromagnetic and Hydrodynamic Equations: Application to Turbulence. Ph.D. Thesis, Brown University, Providence, RI, USA, 1999.
27. Batchelor, G.K. On the Spontaneous Magnetic Field in a Conducting Liquid in Turbulent Motion. *Proc. R. Soc. A* **1950**, *201*, 405.
28. Lieberman, M.A.; Lichtenberg, A.J. *Principles of Plasma Discharges and Materials Processing*; John Wiley & Sons: New York, NY, USA, 1994.
29. RBalescu; Senatorski, A. A new approach to the theory of fully developed turbulence. *Ann. Phys.* **1970**, *58*, 587–624. [[CrossRef](#)]
30. Chen, H.; Kandasamy, S.; Orszag, S.; Shock, R.; Succi, S.; Yakhot, V. Extended Boltzmann kinetic equation for turbulent flows. *Science* **2003**, *301*, 633–636. [[CrossRef](#)] [[PubMed](#)]
31. Biskamp, D. *Magnetic Reconnection in Plasmas*; Cambridge University Press: Cambridge, UK, 2005.
32. Lowes, F.J. Measuring magnetic field in the ‘diamagnetic’ ionosphere. *Geophys. J. Int.* **2007**, *171*, 115–118. [[CrossRef](#)]
33. Schmidt, G. *Physics of High-Temperature Plasmas—An Introduction*; Academic Press: New York, NY, USA, 1966.
34. Bhattacharjee, C. Classifying diamagnetic states of plasma near Schwarzschild event horizon: Local approximation. *Phys. Lett. A* **2020**, *384*, 126698. [[CrossRef](#)]
35. Wang, W.; Liu, R.; Wang, Y.; Hu, Q.; Shen, C.; Jiang, C.; Zhu, C. Buildup of a highly twisted magnetic flux rope during a solar eruption. *Nat. Commun.* **2017**, *8*, 1330. [[CrossRef](#)]
36. Chatwin, P. The vorticity equation as an angular momentum equation. *Math. Proc. Camb. Philos. Soc.* **1973**, *74*, 365–367. [[CrossRef](#)]
37. Okamoto, N.; Davidson, P.A.; Kaneda, Y. On the decay of low-magnetic-Reynolds-number turbulence in an imposed magnetic field. *J. Fluid Mech.* **2010**, *651*, 295–318. [[CrossRef](#)]
38. Zolotarev, M.S.; McDonald, K.T. Diffraction as a consequence of Faraday’s law. *Am. J. Phys.* **2000**, *68*, 674. [[CrossRef](#)]
39. Kline, M. *Electromagnetic Theory and Geometrical Optics*; Research Report No. EM-171; New York University: New York, NY, USA, 1963.
40. Marathay, A.S.; McCalmont, J.F. Vector diffraction theory for electromagnetic waves. *J. Opt. Soc. Am. A* **2001**, *18*, 2585–2593. [[CrossRef](#)]
41. Fujii, M. A new mode of radio wave diffraction via the terrestrial surface plasmons on mountain range. *Radio Sci.* **2016**, *51*, 1396–1412. [[CrossRef](#)]
42. Sreenivasan, K.; Meneveau, C. The fractal facets of turbulence. *J. Fluid Mech.* **1986**, *173*, 357–386. [[CrossRef](#)]
43. Dubief, Y.; Delcayre, F. On coherent-vortex identification in turbulence. *J. Turbul.* **2000**, *1*, 011. [[CrossRef](#)]
44. Zada, I.; Zhang, W.; Li, Y.; Sun, P.; Cai, N.; Gu, J.; Liu, Q.; Su, H.; Zhang, D. Angle dependent antireflection property of TiO₂ inspired by cicada wings. *Appl. Phys. Lett.* **2016**, *109*, 153701. [[CrossRef](#)]
45. Paratore, F.; Boyko, E.; Kaigala, G.V.; Bercovici, M. Electroosmotic Flow Dipole: Experimental Observation and Flow Field Patterning. *Phys. Rev. Lett.* **2019**, *122*, 224502. [[CrossRef](#)] [[PubMed](#)]
46. Tu, N.H.; Yoshioka, K.; Sasaki, S.; Takamura, M.; Muraki, K.; Kumada, N. Active spatial control of terahertz plasmons in graphene. *Commun. Mater.* **2020**, *1*, 7. [[CrossRef](#)]
47. Kim, J.; Han, K.; Hahn, J.W. Selective dual-band metamaterial perfect absorber for infrared stealth technology. *Sci. Rep.* **2017**, *7*, 6740. [[CrossRef](#)]
48. Mouritz, A.P. (Ed.) Polymers for aerospace structures. In *Introduction to Aerospace Materials*; Woodhead Publishing: Sawston, UK, 2012; pp. 268–302.